

Computational Studies on LSM12 as an
NAADP-binding Protein and its Role in
Activating the TPC2 Channel

Candidate Number: 1032271

Word count: 6531

Contents

Abstract	2
Abbreviations	3
1 Introduction	4
1.1 NAADP	4
1.2 TPC2	6
1.3 LSM12	8
1.4 Molecular Dynamics	10
1.5 Molecular Docking	10
1.6 Project Aims	11
2 Materials and Methods	11
2.1 Sequences and Molecular Structures	11
2.1.1 LSM12 and TPC2	11
2.1.2 Ligands	12
2.2 Molecular Dynamics	13
2.2.1 MD Engine and Force Fields	13
2.2.2 System Preparation	14
2.2.3 Production MD	14
2.3 Ligand Docking	15
2.4 Protein-protein Docking	15
2.5 Data analysis and Visualization	16
3 Results	16
3.1 Dynamic Features of NAADP, NADP and TPC2-A1-N	16
3.2 Dynamic Properties of LSM12	18
3.3 Assessment of NAADP-LSM12 Binding	21
3.3.1 Molecular Docking and Initial MD Assessment	21
3.3.2 Extended Simulation of #8	22
3.3.3 Extended Simulation of #14	25
3.3.4 De novo binding simulation	27
3.4 Protein-protein docking	27
4 Discussion	30
References	33

Abstract

Nicotinic acid adenine dinucleotide phosphate (NAADP) is an intracellular signalling molecule that induces release of Ca^{2+} ions from endolysosomes. Several independent studies converged on two-pore channels (TPCs) as the target of action of NAADP, and TPC2 were later found to be involved in a number of human diseases, including fatty liver disease and viral infection, making the NAADP/TPC pathway an emerging druggable target. This pathway also represents an important part of basic cellular biology due to its highly conserved nature in the animal kingdom and the variety of extracellular signals that activate it. However, the absence of an NAADP binding site on TPCs confounded the mechanistic studies on TPCs. It was not until last year that two NAADP-binding proteins required for TPC activation were identified, one of them being LSM12. This pioneering study explores the dynamic features of LSM12 and tries to establish the stable binding mode of NAADP on LSM12 by using a combination of molecular docking and molecular dynamics simulations, in order to guide further elucidation of the mechanisms of TPC2 activation and design of specific small molecule agonist or antagonists of the NAADP/LSM12/TPC2 pathway that might be clinically useful.

Abbreviations

Abbreviation	Meaning
cryo-EM	cryogenic electron microscopy
ER	endoplasmic reticulum
GAFF	general Amber force field
IP ₃	inositol 1,4,5-triphosphate
JPT2	Jupiter Microtubule Associated Homolog-2
LSM12	'like-Sm' protein 12
NAADP	nicotinic acid adenine dinucleotide phosphate
NADP	nicotinamide adenine dinucleotide phosphate
PI(3,5)P ₂	phosphatidylinositol 4,5-bisphosphate
RMSD	root-mean-square deviation
RMSF	root-mean-square fluctuation
RyR	ryanodine receptor
TPC	two-pore channel

1 Introduction

The divalent cation Calcium (Ca^{2+}) is a ubiquitous intracellular signaling messenger that regulates numerous aspects of cellular functions in eukaryotes. Different Ca^{2+} channels localizing to different parts of the cell with distinct regulatory mechanisms and conductivity properties encode “ Ca^{2+} signatures” of specific spatiotemporal patterns, which can then be decoded by the corresponding specific Ca^{2+} sensors and effectors (Luan and Wang, 2021). In animal cells, the functions and mechanisms of Ca^{2+} influx across the plasma membrane, for example through voltage-gated Ca^{2+} channels (Ca_vs), and oscillatory Ca^{2+} release from the large intracellular Ca^{2+} store, endoplasmic reticulum (ER) [sarcoplasmic reticulum (SR) in muscle cells], through inositol 1,4,5-triphosphate receptors (IP_3Rs) and ryanodine receptors (RyRs), have been well established, but the roles of Ca^{2+} release from the small acidic vesicular (endolysosomal) stores, which have a $[\text{Ca}^{2+}]$ comparable to the ER (about $500 \mu\text{M}$) (Morgan et al., 2015), are less well understood (Yang et al., 2019; Raffaello et al., 2016).

Recently, two-pore channels (TPC), transient receptor potential mucolipin channels (TRPML) and P2X4 channels have emerged as the cation channels responsible for Ca^{2+} from the endolysosomal system, of which TPCs in particular have attracted vast research interest after several independent studies converging on TPCs being the target of NAADP (nicotinic acid adenine dinucleotide phosphate) (Brailoiu et al., 2009; Calcraft et al., 2009; Zong et al., 2009), a potent Ca^{2+} -releasing intracellular messenger discovered in 1995 whose target(s) have long remained elusive. Yet, NAADP binding sites were not found on TPCs, and NAADP was shown to bind $\sim 23 \text{ kDa}$ proteins. Subsequent purification and quantitative proteomics identified these small proteins being LSM12 (Zhang et al., 2021) and JPT2 (Gunaratne et al., 2021), and their association with TPCs was also demonstrated.

Elucidation of the mechanisms of TPC activation and endolysosomal Ca^{2+} release will fill the gap in our understanding of this ubiquitous Ca^{2+} mobilization pathway and may contribute to the development of novel therapeutics for human diseases, as endolysosomal Ca^{2+} release through TPCs has been implicated in many physiological functions and related pathological conditions, such as immunity (phagocytosis, inflammatory response and virus trafficking) (Alharbi and Parrington, 2021), cardiac physiology (regulation of SERCA-mediated SR Ca^{2+} uptake, reperfusion after ischaemia, cardiac arrhythmias and hypertrophy) (Terrar, 2022), and cancer (Alharbi and Parrington, 2019). The recent discovery of the accessory proteins involved in this pathway is a major step forward toward this goal, and prompted me to investigate the NAADP/LSM12/TPC2 pathway.

1.1 NAADP

NAADP is a dinucleotide that differs from the common metabolic cofactor, NADP, by replacement of an amide group with a carboxyl group. Its Ca^{2+} mobilizing activity was originally found in sea urchin oocytes (Lee and Aarhus

(1995)) and subsequently found in a wide range of species, including humans, in the animal kingdom (Table 2). NAADP is very potent, being effective at nanomolar concentrations, but it also inhibits Ca^{2+} release at high (micromolar) concentrations, thus exhibiting a bell-shaped dose-response relationship (Morgan and Galione, 2008; Zong et al., 2009).

Table 2: NAADP-evoked Ca^{2+} mobilization has been demonstrated in a wide range of animals.

Cell Type	Reference
Sea urchin oocyte	Lee and Aarhus (1995)
Starfish oocyte	Santella et al. (2000)
Mouse pancreatic acinar cells	Cancela et al. (1999)
Rabbit cardiomyocytes	Bak (2001)
Human T lymphocytes	Berg et al. (2000)

Soon it was discovered that NAADP selectively releases Ca^{2+} from acidic stores, i.e. endolysosomes, in pancreatic acinar and β cells (Yamasaki et al., 2004), myometrial cells (Soares et al., 2007), arterial smooth muscle cells (Kinnear et al., 2004). These studies demonstrated that, both the lysosomal H^+ -ATPase inhibitor baflomycin-A1, which indirectly inhibits lysosomal Ca^{2+} accumulation via $\text{Ca}^{2+}/\text{H}^+$ exchangers, and the lysosomotropic agent glycyphenylalanine-2-naphthylamide (GPN), which causes lysis of lysosomes, abolished the Ca^{2+} -mobilization capability of NAADP but not that of IP_3 or cADPR. They also showed the insensitivity of NAADP-induced Ca^{2+} release to the SERCA (sarco/endoplasmic reticulum Ca^{2+} ATPase) inhibitor thapsigargin that depletes ER Ca^{2+} stores.

Although a few studies found NAADP to be activating RyR1 in the ER in T-lymphocytes, in most other cell types the endolysosomes are consistently involved in independent studies, which led to the discovery of the endolysosome-localized TPC channels that soon became the most promising target of NAADP (see Section 1.2).

Activation of a number of cell surface receptors, such as endothelin-1 (Kinnear et al., 2004), cholecystokinin (Cosker et al., 2010), glutamate (Pandey et al., 2009), glucose (Yamasaki et al., 2004), and histamine (Soares et al., 2007) receptors, in a wide range of mammalian cell types, have been shown to elevate cytosolic NAADP levels, as measured using radioreceptor assays (Churamani et al., 2004). Despite these discoveries, the biosynthetic pathway(s) that are responsible for the production of NAADP, and the upstream signaling cascade following activation, are vague. Although CD38 has been shown to produce NAADP from NADP via a base-exchange reaction in vitro (Aarhus et al., 1995) and in lysosomes (Fang et al., 2018) with nicotinic acid supplied under acidic pH, it is unclear how NAADP could be transported to the cytosol, and CD38

is not required for NAADP production in all cell types (Soares et al., 2007). NADPH oxidases (NOX) or dual NADPH oxidases (DUOX) were shown to produce NAADP from its reduced form, NAADPH during T-lymphocyte activation (TCR/CD3 stimulation), but it is not clear whether this pathway is specific to T-lymphocytes and the sources of NAADPH is still undefined (Gu et al., 2021).

1.2 TPC2

TPCs (two-pore channels) were originally discovered through its sequence homology with voltage-gated Na^+ and Ca^{2+} channels (Na_v and Ca_v) (Ishibashi et al., 2000), and were named after the fact that each TPC protein has two pore-forming domains. Three isoforms (TPC1, TPC2 and TPC3) are found in animals and one (TPC1) was found in plants, all displaying different localization patterns, activation mechanisms and ion selectivity. Like Na_v and Ca_v , TPC channels are pseudotetramers, where each of the four Shaker-like domains contains 6 transmembrane helices (S1-S6), of which S1-S4 constitute a voltage-sensing region and S5-S6 line the pore. Whilst a single Na_v or Ca_v peptide contains all the four domains, each TPC peptide contains two, so that they form a functional channel as a homodimer, and is thus suggested to be an evolutionary intermediate from tetrameric one-domain channels to monomeric four-domain channels (Rahman et al., 2014) (Figure 1). Despite having a voltage-sensor region, TPC2 has lost voltage sensitivity, and either NAADP or $\text{PI}(3,5)\text{P}_2$ (phosphatidylinositol 4,5-bisphosphate) alone can activate it.

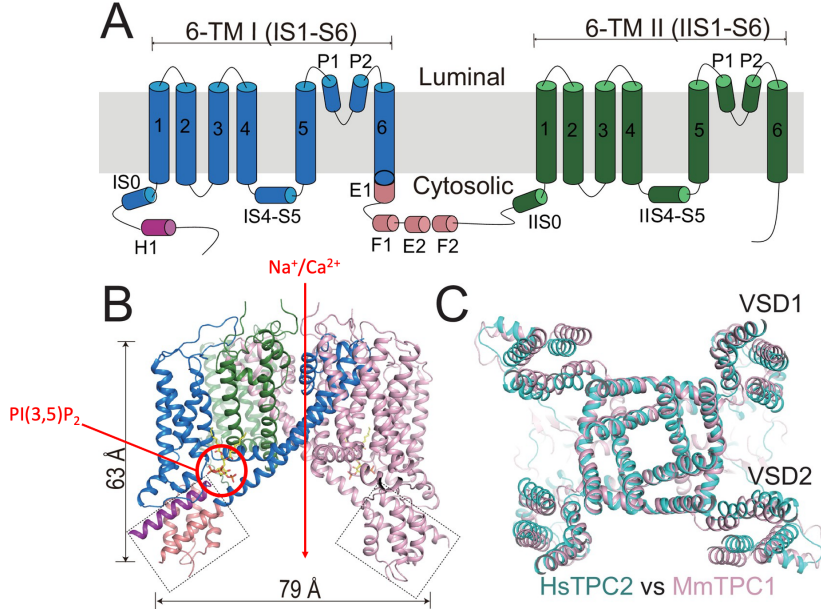


Figure 1: Human TPC2 structure. (A) Topology and domain arrangement of a TPC2 subunit. (B) Cryo-EM strucure of Human TPC2 in its PI(3,5)P₂-bound form (PDB Code: 6NQ0). (C) Human and mouse TPC2 viewed from the top. Adapted from Figure 1, She et al. (2019).

In 2009, three independent studies consistently found TPC1 (Brailoiu et al., 2009) and TPC2 (Calcraft et al., 2009; Zong et al., 2009) to be involved in mediating NAADP-activated Ca²⁺ release by NAADP. Additional studies showed TPC2 to be a better candidate for this role than TPC1. For example, Ruas et al. (2015) detected NAADP-induced Ca²⁺ release in TPC1-knockout mouse embryonic fibroblasts but not TPC2-knockout cells, and re-expression of TPC2 rescued the response. This was further supported by studies on pulmonary arterial myocytes from TPC2-knockout mice (Ogunbayo et al., 2018). By analysing co-localization with markers for different organelles, TPC1 is predominantly expressed in endosomes and TPC2 in lysosomes (Calcraft et al., 2009). Thus, the notion that NAADP releases Ca²⁺ through TPC2 is in accordance with previous finding that NAADP releases Ca²⁺ from acidic stores, particularly lysosomes (see Section 1.1). TPC2 is also particularly interesting due to its implications in diseases such as Parkinson’s disease (Hockey et al., 2015), fatty liver disease (Grimm et al., 2014), and Ebola infection (Yasuteru et al., 2015), as reviewed by Patel and Kilpatrick (2018). Although some studies demonstrated involvement of RyRs in NAADP-induced Ca²⁺ release, only in T-lymphocytes and pancreatic acinar cells is there strong evidence that RyR1 is the primary channel activated by NAADP and in other cell types RyRs may only serve to amplify

Ca^{2+} signal by Ca^{2+} induced Ca^{2+} release (CICR) (Roggenkamp et al., 2021). Indeed, in most cell types, TPC2 overexpression, knockdown and electrophysiological studies support their role in NAADP-mediated Ca^{2+} release (reviewed by Walseth and Guse (2021)).

However, later electrophysiological studies by patch-clamp on isolated endolysosomes (Wang et al., 2012), plasma membrane (Guo et al., 2017) or baker's yeast giant vacuoles (Boccaccio et al., 2014) containing native or redirected TPCs suggested TPC1 and TPC2 to be Na^+ channels activated by $\text{PI}(3,5)\text{P}_2$, with structural mechanisms further described using cryo-EM (She et al., 2018, 2019).

These seemingly contradictory findings led to the hypothesis that TPCs might change ion selectivity depending on the agonist. This notion is strongly supported by a recent study, where the effects on TPC2 of NAADP, $\text{PI}(3,5)\text{P}_2$, and their corresponding membrane-permeable small-molecule mimics, TPC2-A1-N and TPC2-A1-P, were compared using electrophysiological methods. Importantly, by measuring the reversal potential under bi-ionic conditions, the permeability ratio, $P_{\text{Ca}^{2+}}/P_{\text{Na}^+}$, can be calculated from the Goldman–Hodgkin–Katz equation. Accordingly, NAADP and TPC2-A1-N were found to induce a much higher $P_{\text{Ca}^{2+}}/P_{\text{Na}^+}$ (about 0.65) than $\text{PI}(3,5)\text{P}_2$ and TPC2-A1-P (about 0.04) (Gerndt et al., 2020). The former is consistent with that measured previously by endo-lysosomal patch-clamp under NAADP activation ($P_{\text{Ca}^{2+}}/P_{\text{Na}^+}=0.6\text{--}0.8$) (Ruas et al., 2015). Thus, it would be interesting to investigate how the mode of TPC2 opening is different when activated by $\text{PI}(3,5)\text{P}_2$ /TPC2-A1-P or by NAADP/TPC2-A1-N.

1.3 LSM12

Despite mounting evidence that TPC1 and TPC2 are the targets of NAADP, an NAADP binding site on TPCs was not found. Photoaffinity labeling using radioactive NAADP derivates resulted in specific labeling of 41-kDa proteins in sea urchins and 22–23 kDa proteins in mammalian cells (Lin-Moshier et al., 2012; Gunaratne et al., 2019), with high affinity and selectivity for NAADP over NADP (8–15 fold; Lin-Moshier et al. (2012)). These putative NAADP-binding proteins, which are much smaller than TPCs, were recently purified and identified, using mass spectrometry, to be Jupiter Microtubule Associated Homolog-2 (JPT2), in human erythrocytes (Gunaratne et al., 2021) and T-lymphocytes (Roggenkamp et al., 2021), and ‘like-Sm’ protein 12 (LSM12) in human embryonic kidney (HEK) 293 cells (Zhang et al., 2021). JPT2 co-immunoprecipitates with TPC1 (Gunaratne et al., 2021) and RyRs (Roggenkamp et al., 2021), and LSM12 co-immunoprecipitates with both TPC1 and TPC2 (Figure 2).

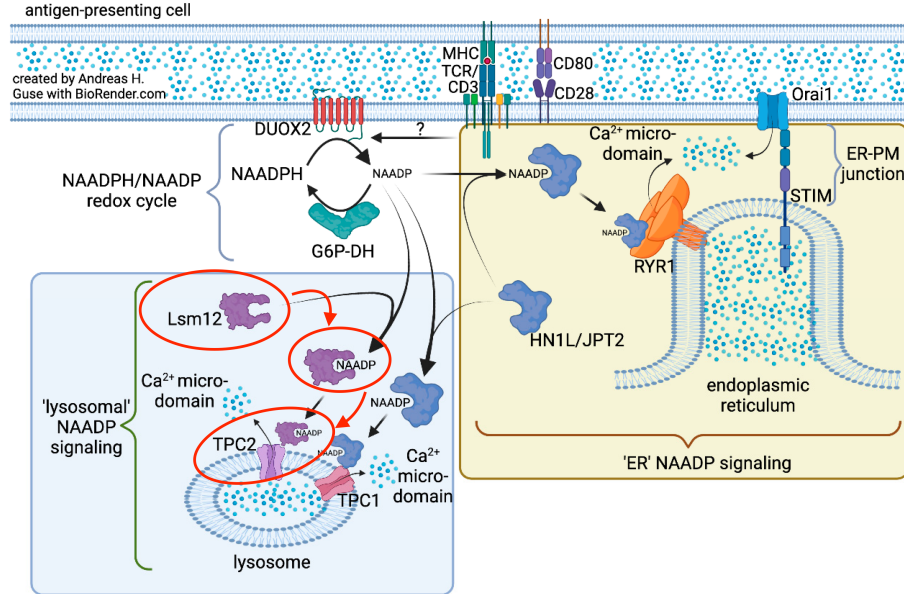


Figure 2: Current knowledge about mechanisms of NAADP-induced Ca^{2+} release. The NAADP/LSM12/TPC2 pathway is highlighted in red. The ER pathway has been mostly demonstrated in the context of T-cell activation whilst most other cell types seem to employ the lysosomal pathway, in which TPC2 has been shown to be the most prominent channel involved. The identification of accessory proteins help to explain the different responses to NAADP in different cell types. Adapted from Figure 2, Guse (2022).

LSM12 binds to NAADP directly with an estimated K_d of ~30 nM, and NADP up to 100 μM barely disrupts LSM12-NAADP binding. LSM12 is required for NAADP-evoked Ca^{2+} release in HEK293 cells, as demonstrated by a LSM12-knockout cell line. It has an N-terminal LSM domain (residues 4-67) and a putative C-terminal anticodon-binding (AD) domain (residues 68-84) joined by a linker (residues 68-84). Truncation mutants ΔLsm abolished association to NAADP and TPC2, whereas ΔAD and Δlinker were nearly as functional as the intact LSM12, meaning the LSM domain are both responsible for NAADP binding and TPC2 activation (Zhang et al., 2021). Recently it was shown that LSM12 also competitively antagonizes the effect of $\text{PI}(3,5)\text{P}_2$ on TPC2 (Du et al., 2022), which means LSM12 might make the distinction between the two modes of TPC2 activation (by NAADP or $\text{PI}(3,5)\text{P}_2$; see Section 1.2) more significant.

1.4 Molecular Dynamics

Molecular dynamics aims to simulate the evolution of a chemical system and logs the changes in the positions of the atoms in the system over time in a trajectory file. While quantum mechanics (QM) more accurately describes the behavior of atoms, the complexity of QM and semi-QM calculations, which deals with electrons, limits their use to small molecules. To make simulation of a system containing, in this case, tens of thousands of atoms feasible, molecular dynamics use force fields to approximate the behavior of atoms as a function of their nuclear positions only (Leach and Leach, 2001).

A force field includes a functional form which defines the potential energy of a system. The simplest form, as shown below, includes bonded interactions (bond stretching, angle bending, torsional angles) and non-bonded interactions (Lennard-Jones potential for van der Waals interactions and Coulomb potential for electrostatic interactions). The force field also includes the constants and atom type-specific reference parameters, and these vary among different force fields even if the functional forms are similar (Leach and Leach, 2001).

$$V(r^N) = \sum_{i \in \text{bonds}} k_{bi}(l_i - l_i^0)^2 + \sum_{i \in \text{angles}} k_{ai}(\theta_i - \theta_i^0)^2 + \sum_{i \in \text{torsions}} \frac{V_i^n}{2}[1 + \cos(n\omega_i - \gamma_i)] \\ + \sum_{i=1}^N \sum_{j=i+1}^N \left(4\epsilon_{ij} \left[\left(\frac{r_{ij}^0}{r_{ij}} \right)^{12} - 2 \left(\frac{r_{ij}^0}{r_{ij}} \right)^6 \right] + \frac{q_i q_j}{4\pi\epsilon_0 r_{ij}} \right)$$

With potential energy calculated and atomic positions known, the motion of atoms can be calculated repeatedly with a timestep on the order of femtoseconds by solving differential equations according to classical mechanics (Newton's second law) (Leach and Leach, 2001).

In this study, MD simulations are used to generate a range of conformations of LSM12 to which NAADP would be docked, and to verify the stability of NAADP-LSM12 complexes.

1.5 Molecular Docking

Molecular docking aims to establish the stable binding mode(s) between a ligand and a receptor, where the receptor is a protein and the ligand is usually another protein, small molecule, or nucleic acids. To do so, different binding poses of the ligand are generated, whose binding affinities are then estimated and ranked using scoring functions. There are a number of different approaches to conformation sampling and scoring, as reviewed by Meng et al. (2011) and Guedes et al. (2018).

In this study, molecular docking of NAADP to LSM12 was initially used as a rough guide of where the potential binding sites would be, and promising

binding poses were subsequently verified for their stability by MD simulations. Docking of LSM12 to TPC2 were also attempted.

1.6 Project Aims

The LSM12 is one of the first discovered NAADP-binding protein and is a key accessory protein mediating NAADP-induced activation of TPC2 channel. Due to its recent discovery, there is a lack of understanding of the structural details of its interaction with NAADP and TPC2. Thus, this project aims to:

1. Establish the stable binding mode(s) of NAADP on LSM12
2. Explore how NAADP-LSM12 binding affects the dynamic properties of LSM12, and suggest how this might promote LSM12-TPC2 binding and activation
3. Compare the effect of NAADP with that of the ineffective mimic NADP and the more potent mimic TPC2-A1-N

2 Materials and Methods

2.1 Sequences and Molecular Structures

2.1.1 LSM12 and TPC2

LSM12 does not have an experimentally solved structure, so an AlphaFold-predicted structure of the human LSM12 (UniProt ID: Q3MHD2) was used. The PDB structure file, which was created with the AlphaFold Monomer v2.0 pipeline (Jumper et al., 2021; Varadi et al., 2022) on July 2021, was downloaded from AlphaFold DB version 1¹.

¹<https://alphafold.ebi.ac.uk/entry/Q3MHD2>

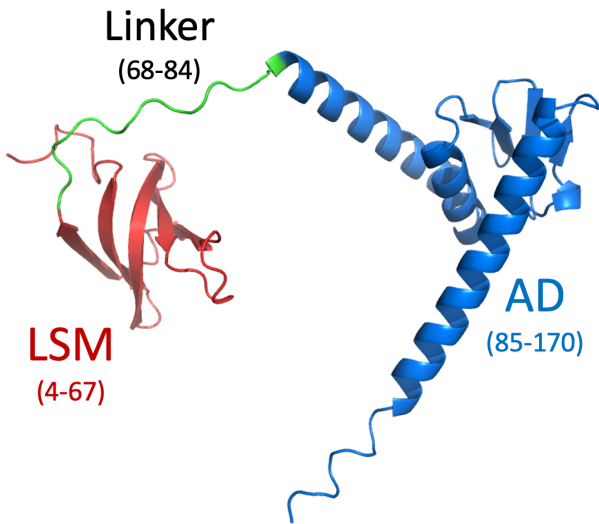


Figure 3: The AlphaFold-predicted structure of LSM12 with annotated domain arrangement according to Zhang et al. (2021).

Since the LSM domain is the functional domain (see Section 1.3), most docking and simulation experiments are conducted using the truncated version of LSM12 containing the first 80 residues, which is referred to as LSM12¹⁻⁸⁰ (or “LSM” in some plot titles).

The Cryo-EM structure of human TPC2 channel in the apo state (PDB code: 6NQ1) was used in LSM12-TPC2 docking experiments [She-2019].

2.1.2 Ligands

The ideal structure of NAADP was downloaded from the RSCB Protein Data Bank² (ligand ID: DN4) as an .sdf file which was converted to the .mol2 format using Open Babel Version 3.1.1 (O’Boyle et al., 2011), then deprotonated by manual editing using PyMOL, so that the structure conforms to that shown in Fig. 4.

²<https://www.rcsb.org>

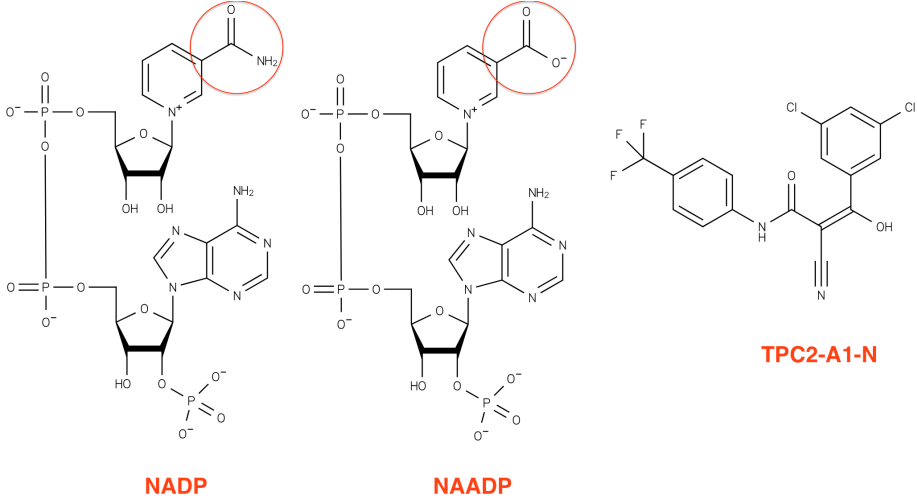


Figure 4: The structural formulae of the ligands used in docking and MD simulations. Red circles highlight the difference between NADP and NAADP.

Since LSM12 and TPC2 are not sensitive to NADP (Zong et al., 2009; Zhang et al., 2021), NADP is used as a negative control. An NADP structure was downloaded (ligand ID: NAP) and processed similarly, which was used to run ligand-alone MD simulations. When NADP was used as a control for NAADP in protein-ligand simulations, each NADP structure was generated from the corresponding NAADP structure by a personal script that converts the amide group to a carboxyl group without altering the coordinates of the atoms for the rest of the molecule.

TPC-A1-N was generated by drawing the molecule in PlayMolecule Parameterize³ and downloading the structure in .mol2 format.

2.2 Molecular Dynamics

2.2.1 MD Engine and Force Fields

All MD simulations were performed using GROMACS (version 2020.3) (Abraham et al., 2015). The protein component was parameterized with the Amber ff14SB force field (Maier et al., 2015). The TIP3P model was selected for the water solvent (Jorgensen et al., 1983). Where ligands (NAADP/NADP/TPC2-A1-N) were present in the system, they were parameterized using antechamber with the GAFF force field (Wang et al., 2004), and the output is converted to GROMACS-compatible topology files using acpype (Sousa da Silva and Vranken, 2012).

³<https://www.playmolecule.com/parameterize>

2.2.2 System Preparation

In all simulations, the solute (protein, ligand, or both) was placed at the center of a dodecahedron box with a minimum distance of 1.0 nm to box boundaries. The box was solvated with water molecules using the TIP3P model and Na^+ and Cl^- ions were randomly added to achieve overall charge neutrality and a physiological 0.15 M salt concentration (Figure 5).

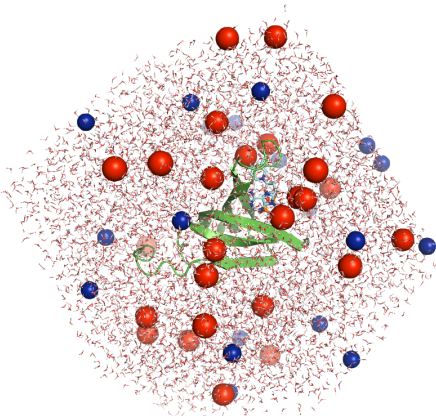


Figure 5: A GROMACS simulation box containing LSM12¹⁻⁸⁰ (green), NAADP (cyan), solvent (water) and neutralizing ions: Na^+ (red) and Cl^- (blue).

The system is then energy minimized using the steepest descent method with target maximum force of $1000 \text{ kJ mol}^{-1} \text{ nm}^{-1}$ to relax any steric clashes or inappropriate geometry. This is then followed by a 1.0 ns isothermal-isochoric (NVT) equilibration at 300 K using the velocity-rescale thermostat (Bussi et al., 2007), and subsequently a 1.0 ns (isothermal-isobaric) NPT equilibration with a reference pressure of 1 bar using the Berendsen barostat (Berendsen et al., 1984).

2.2.3 Production MD

Simulations of each system, which contains LSM12, a ligand, or both, were run for at least 100 ns. Some simulations were extended to different lengths, which are noted in the Results section. The parameters used were the same as in NPT equilibration except that the position restraints applied in NVT and NPT equilibration were released and the Parrinello-Rahman barostat (Parrinello and Rahman, 1981) was used.

2.3 Ligand Docking

Conformation sampling was performed using PLANTS (Korb et al., 2006). Since the binding site of NAADP on LSM12¹⁻⁸⁰ is unknown, blind sampling of 1000 NAADP conformations was performed within a sphere whose radius is 40 Å and origin is located at the backbone N of Glu28 near the center of LSM12¹⁻⁸⁰ (Figure 6). Because the receptor (LSM12¹⁻⁸⁰) is considered as rigid during molecular docking, to account for its flexibility, NAADP was docked onto a number of post-MD conformations of LSM12¹⁻⁸⁰.

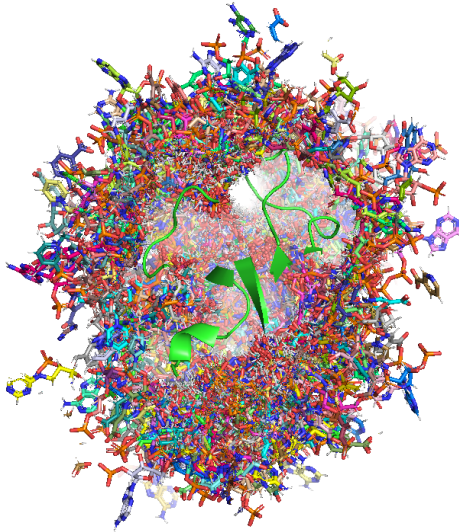


Figure 6: 1000 poses of NAADP docked on to LSM12¹⁻⁸⁰.

The scoring was performed using Amber MM/GBSA (molecular mechanics energies combined with the generalized Born and surface area continuum solvation) (Genheden and Ryde, 2015), a force field-based scoring function. The ff14SB and GAFF force fields were used to describe the protein and the ligand, respectively, and the solvent was implicitly described as a continuum.

2.4 Protein-protein Docking

Docking of LSM12¹⁻⁸⁰ to TPC2 was performed using HADDOCK 2.4 (Zundert et al., 2016). Selection of ‘active residues’—those involved in the interaction between the two proteins—was biased towards the interacting residues in a LSM12-TPC2 complex produced using ClusPro (another protein-protein docking tool), by T. Rahman (personal communication, 2021; see Section 3.4).

2.5 Data analysis and Visualization

For data extraction from MD simulation trajectories, root-mean-square deviation (RMSD) and root-mean-square fluctuation calculations were performed using GROMACS programs `gmx rms` and `gmx rmsf`, respectively. Distance measurements were performed using MDAnalysis (Michaud-Agrawal et al., 2011).

Statistical analysis were performed using R⁴, diagrams were plotted using ggplot2 (Wickham, 2016), and PyMOL⁵ was used for molecular visualization.

3 Results

3.1 Dynamic Features of NAADP, NADP and TPC2-A1-N

The intrinsic dynamic conformational properties of NAADP, NADP, and TPC2-A1-N may be responsible for their different affinities to LSM12. Thus, a 1000 ns MD simulations was performed on each of these ligands.

To access the stability of each ligand, the RMSD of the non-H atoms the ligand in 100,000 frames uniformly extracted from the 1000 ns simulation was calculated relative to that at start of the simulation (the NPT-equilibrated structure). RMSD of each frame indicates the structural similarity of the molecule relative to the NPT-equilibrated reference structure, thus can be used to quantify the structural stability of the ligand throughout the simulation.

As shown in Figure 7, while NAADP and NADP both significantly deviate from the initial conformation and show some degree of fluctuation, TPC2-A1-N conforms to the initial structure and remains rigid, and this trend continues throughout the 1000 ns simulation (only the first 100ns is shown so as to reveal fluctuation patterns of NAADP and NADP clearly). NAADP and NADP are both flexible, with the distance between the two aromatic rings (inter-ring distance) ranging from 4Å to 18Å. TPC2-A1-N, by contrast, is rigid (Figure 7 (C)). Inter-ring distances were measured for NAADP and NADP throughout the 1000 ns simulation. This reveals that NAADP is more flexible than NADP (Figure 8 (A, B)), and while NADP is more likely to adopt a folded conformation, NAADP is more likely to adopt an extended conformation (Figure 8 (C, D)). In NADP, the amide group co-planar with the aromatic ring might facilitate attraction to the other aromatic ring via delocalized π electron interactions whereas in NAADP, polar-charge interactions between the carboxyl group and water molecules may disrupt this π stacking, thus accounting for its flexibility and tendency to adopt an extended conformation.

⁴<https://www.r-project.org/>

⁵<https://pymol.org>

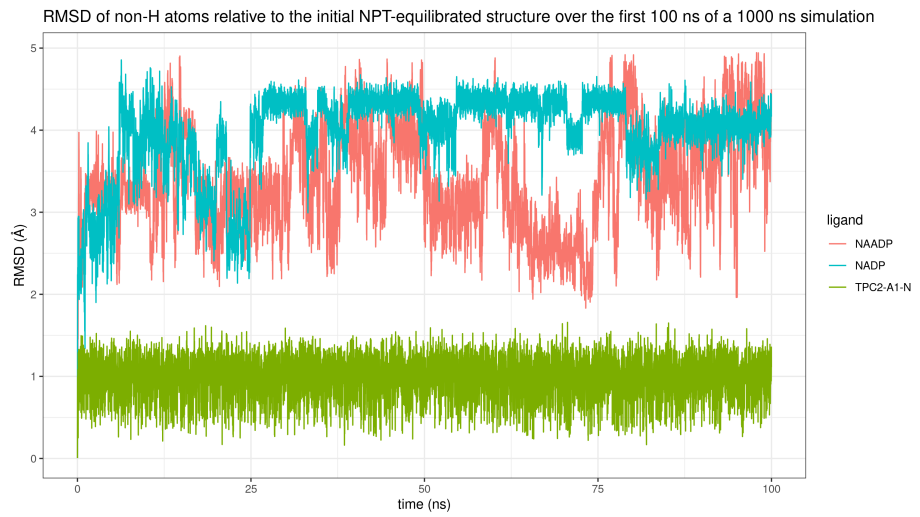


Figure 7: RMSD of non-H atoms relative to the initial NPT-equilibrated structure over the first ns of a 1000 ns simulation of NAADP, NADP or TPC-A1-N.

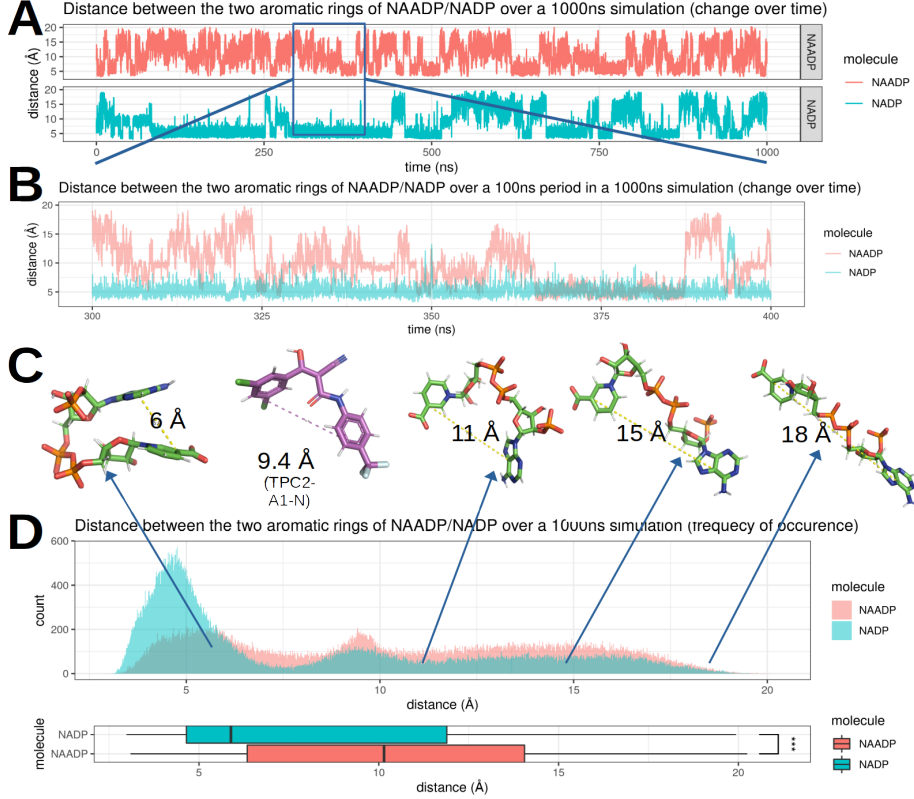


Figure 8: Dynamic properties of NAADP and NADP during a 1000ns-long simulation. (A) Change over time of the distance between the two aromatic rings. (B) A zoomed-in view of (A) corresponding to the 100ns period from 300ns to 400ns. (C) Representative 3D conformations of NAADP (NADP) with different inter-ring distances. The rigid conformation of TPC2-A1-N is also included for comparison. (D) Distribution of the inter-ring distance of NAADP or NADP based on 100,000 frames extracted from a 1000 ns-long simulation. The median distance is 10.1 Å and 5.89 Å for NAADP and NADP, respectively; mean distance, 10.4 Å and 8.25 Å. The significance of difference is tested using two-tailed t test, which yielded $p < 2.2 \times 10^{-16}$.

3.2 Dynamic Properties of LSM12

7 independent 100 ns simulations of LSM12 using the AlphaFold structure as the starting structure showed that the LSM and AD domains are relatively stable, but they do not stably associate with each other in a specific manner due to the flexible linker. This, in addition to Zhang et al. (2021)'s finding that the LSM domain alone is functional, justifies the use of the truncated version, LSM12¹⁻⁸⁰,

in subsequent studies, as the entire surface of the LSM12 is free to interact with TPC2 and NAADP (Figure 9).

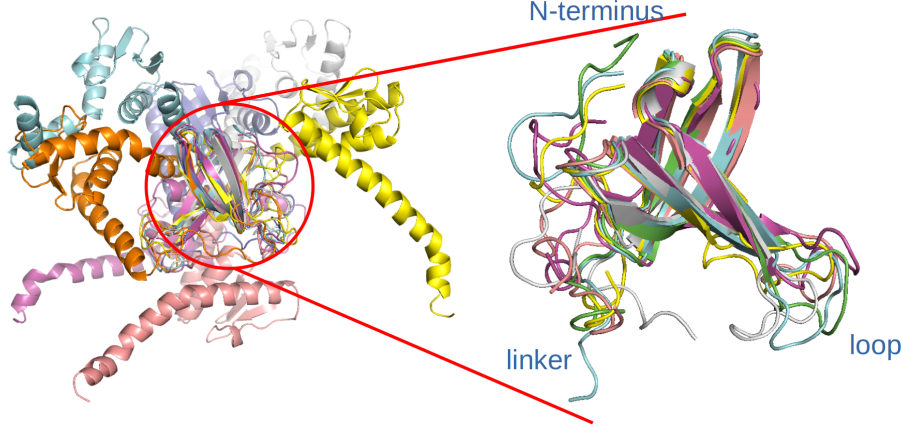


Figure 9: The structures of LSM12 at the end of 100 ns simulations, with structural alignments performed on the LSM domain. A zoomed-in view of the final truncated LSM12¹⁻⁸⁰ structures is shown on the right.

4 additional 100ns simulations were run for LSM12¹⁻⁸⁰ (Run 1 was extended to 1000 ns), and average root-mean-square fluctuation (RMSF) for each residue was calculated, allowing quantification of the displacement of each residue from their average positions (Figure 10). It is evident from the RMSF plot that the β -barrel core of LSM12¹⁻⁸⁰ is relatively stable, while the loop between residues 44-53, the linker beyond residue 70, and the N-terminal residues (1-10) are flexible, consistent with simulations on intact LSM12 (Figure 9).

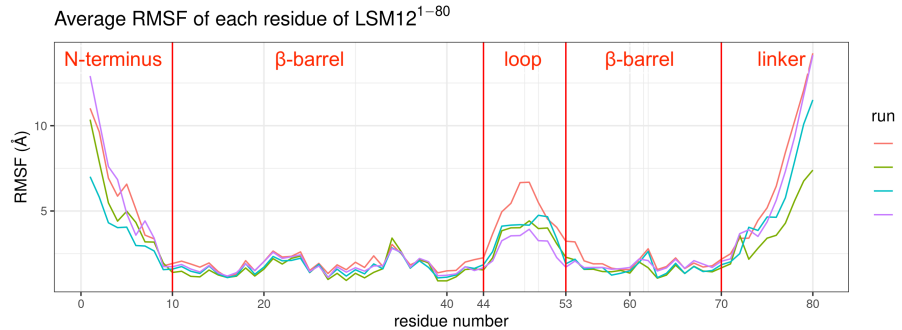


Figure 10: Average RMSF of each residue of LSM12¹⁻⁸⁰ during 4 independent MD simulations.

The distance between the loop and the linker was measured in order to roughly quantify their stability and the state of the groove between them. The distance between the center of mass of the loop (residues 44-53) and that of first 6 residues (70-75) of the linker were defined as the loop-linker distance (Figure 11 (A)). In 4 independent 100 ns simulations of LSM12¹⁻⁸⁰ starting from the truncated AlphaFold structure, the loop-linker distance showed wide ranges of distribution and averages at about 20-21 Å (Figure 11 (B)) which was slightly reduced to 18.9 Å in the extended 1000 ns simulation (Figure 11 (C)). The loop and the linker did not converge to a stable conformation after 1000 ns of simulation, further supporting its flexible nature (Figure 11 (D)).

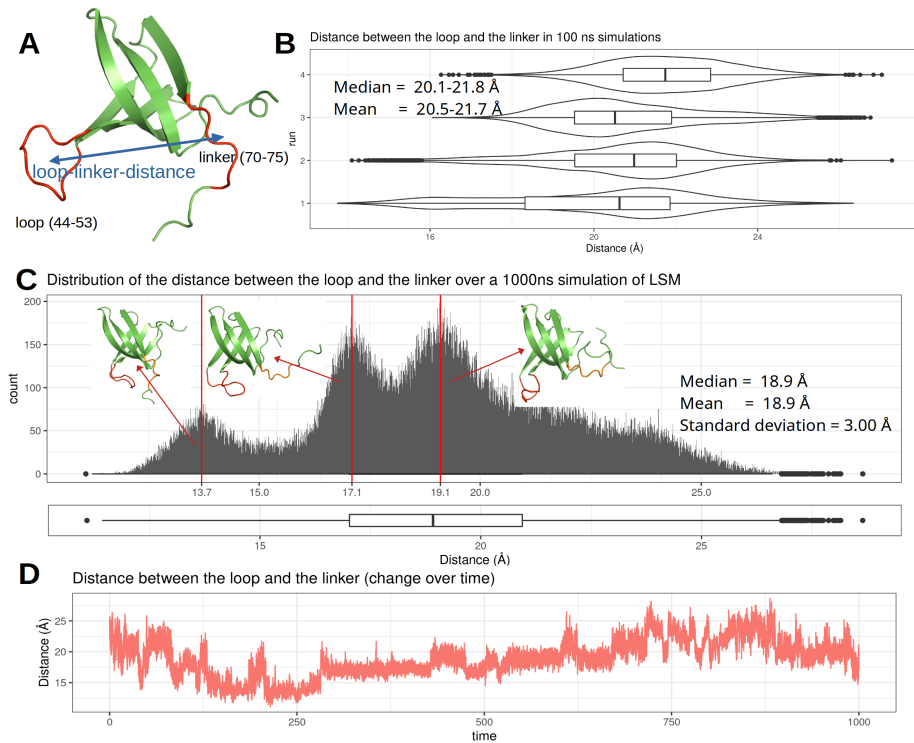


Figure 11: The flexible nature of the loop and linker of LSM12¹⁻⁸⁰. (A) A demonstration of ‘loop-linker’ distance. (B) Distribution of loop-linker distance in 4 independent 100 ns simulations of LSM12¹⁻⁸⁰ using the AlphaFold structure as the starting point. (C) Distribution of loop-linker distance during an extended 1000 ns simulation (100,000 frames extracted), labelled with representative conformations. (D) Change over time of the loop-linker distance in an 1000 ns simulation.

NADP—and indeed most other nucleotide cofactors—usually binds to a rela-

tively deep pocket in the protein and is often enclosed by a flexible loop, for example, as in PDB structures 1D4O, 1GVE, 1HET and 1J96. However, such prominent binding pocket is not evident by examining the surface of LSM12¹⁻⁸⁰ (not shown). The only way such a groove can be formed is by induced-fitting of flexible regions initiated by NAADP binding, and indeed, as shown by MD simulations of LSM12¹⁻⁸⁰ complexes (Section 3.3.1), NAADP tends to stably associate with the groove between the loop and the linker.

3.3 Assessment of NAADP-LSM12 Binding

3.3.1 Molecular Docking and Initial MD Assessment

77 post-MD conformations of LSM12¹⁻⁸⁰ were extracted from the 7 independent 100 ns simulations of LSM12 at 90-100 ns with an interval of 1 ns. 1000 poses of NAADP were docked onto each of these LSM12¹⁻⁸⁰ structure, totaling 77,000 NAADP poses. Amber MM/GBSA scores were calculated for these poses and used to rank them, and the top 10 highest-scoring complexes were each subject to a 100 ns simulation (Figure 12 (#1-10)). It turns out that high-scoring conformations are not always stable, but a common feature of stable conformations (#1, #5, #7 and #8, as highlighted in red rectangles) is the close association between NAADP and the loop.

In addition, 3000 poses of NAADP were docked on to the LSM12 conformation that was extracted from a ClusPro-generated TPC2-LSM12 complex (T. Rahman, personal communication; see Section 3.4), and 5 manually selected conformations, which had relatively high GBSA scores and were close to the loop, were similarly subject to 100 ns simulations (Figure 12 (#11-15)). Two of these conformations (#13 and #14) were relatively stable.

#8 and #14 were extended to assess their stability over a longer timescale and their effects on LSM12¹⁻⁸⁰ conformation.

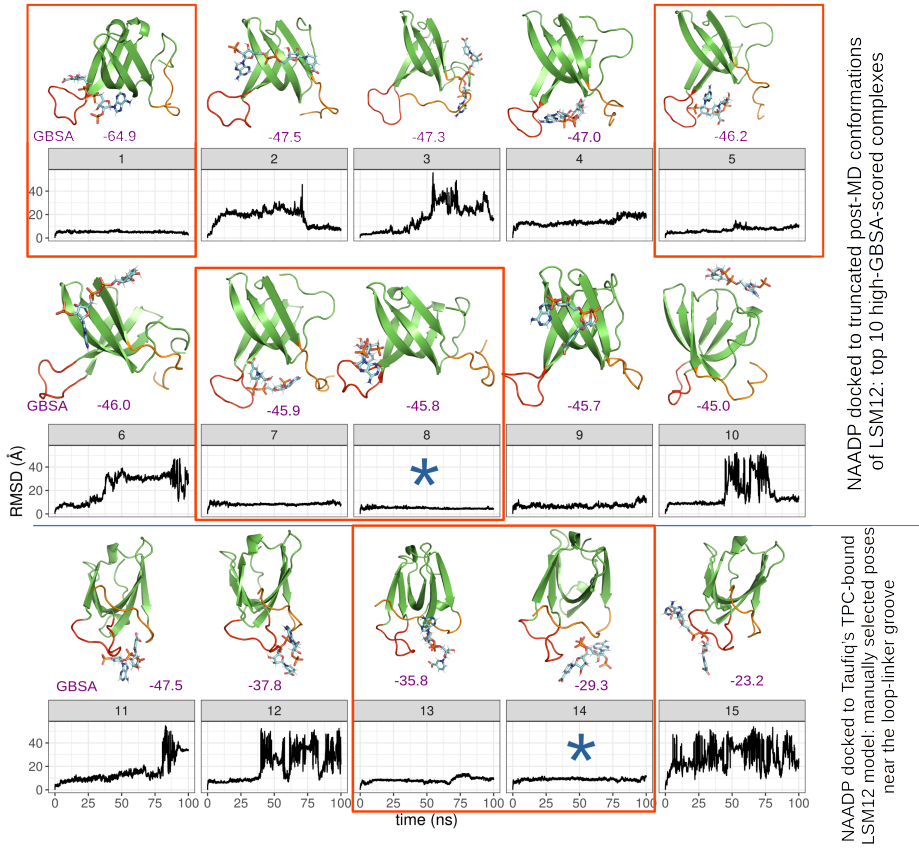


Figure 12: MD simulations of promising $LSM12^{1-80}$ -NAADP complexes. Purple numbers are Amber MM/GBSA scores (in $\text{kJ} \cdot \text{mol}^{-1}$). Line plots show RMSD of NAADP with reference to the initial binding pose at 0 ns (the NAADP position was normalized with respect to $LSM12^{1-80}$). Red rectangles highlight stable complexes. Simulations labelled with blue asterisks (*) were later extended.

3.3.2 Extended Simulation of #8

1900 ns extended simulation of #8 revealed unbinding of the initial unstable pose, rebinding to the loop-linker groove, and the association to this site for more than 1500 ns (Figure 13 A). The initial NAADP pose obtained from molecular docking was located at the groove between the loop and the β -barrel, and the the loop was separated far from the linker (Figure 13 (D1)). Despite the favorable Amber MM/GBSA docking score, this conformation was unstable, where NAADP switched between folded and extended conformations frequently (the plot is smoothed due to the use of the rolling average of 10 frames, but the

high degree of fluctuation is evident from the standard deviation of 2.81 Å) and eventually dissociated from LSM12¹⁻⁸⁰ at 252 ns (Figure 13 (A, B, D3)). Nevertheless, during this unstable period, NAADP seemed to promote the association between the loop and the linker by attracting Arg72 on the linker towards the loop via its phosphate groups (Figure 13 (D2, F)).

After reaching as far as 40 Å away from LSM12¹⁻⁸⁰, NAADP rebound to LSM12¹⁻⁸⁰ at the loop-linker groove at 320 ns in its folded conformation, and since then it never dissociated from the groove again during the rest ~1500 ns of the simulation (Figure 13 (A, B)). NAADP largely remained in its folded conformation between 320 and 670 ns, but with relatively high fluctuations (Figure 13 B). The stabilizing interactions during this period include the electrostatic interactions between Arg72 and the phosphates, and the enthalpy-driven proline-aromatic interactions (Zondlo, 2013) between Pro50 and the purine ring (Figure 13 (D4); all residues on the loop and the linker are shown to illustrate that no other favorable interactions are evident).

NAADP experienced a structural rearrangement at 670 ns and maintained its L-shaped conformation since then (Figure 13 (B)). From 670 to about 850 ns, the Arg72-phosphate and P50-purine interactions persisted but since the rotational rearrangement of NAADP near 866 ns, the electrostatic interaction between Arg72 and the carboxyl group of nicotinate became the dominant attractive interaction (Figure 13 (D5/6)), and the distance from the central carbon of the guanidium group to the nearest oxygen on the carboxyl group averaged at 3.77(±0.86) Å (Figure 13 (E)) until 1250 ns, when another rearrangement occurred and the Arg72-carboxyl interaction becomes destabilized (Figure 13 (D7, E)). It is curious why Glu74 was almost constantly in close contact with the phosphate groups since 320 ns (Figure 13 (D4/6/7)) and yet did not promote NAADP to unbind in this simulation, even when stabilizing interactions were less prominent (Figure 13 (D7)).

The distance between the loop and the linker showed a general descending trend (from 21.3 Å to 13-14 Å) and with decreasing fluctuation throughout the simulation, supporting that the NAADP binding was associated to, if not causing, groove closing and stabilization.

LSM12¹⁻⁸⁰ and NAADP conformations were extracted at 900 ns, and additional two 100 ns simulations were run, both of which failed to reproduce the stable binding at the loop-linker groove, as NAADP either unbound completely or drifted to a different site on the surface of LSM12¹⁻⁸⁰ (not shown).

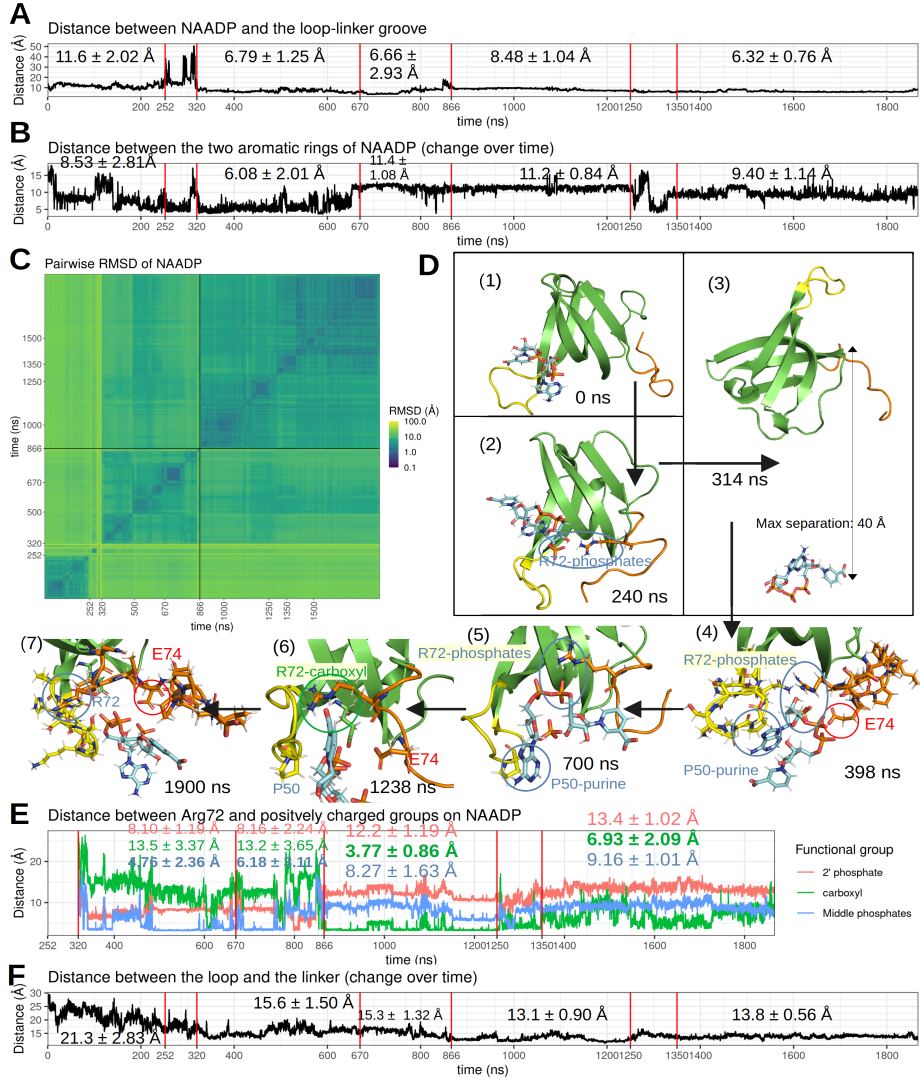


Figure 13: 1900 ns extended simulation of #8. (A) Distance between the center of mass of NAADP and that of the loop-linker groove over time. (B) Distance between the two aromatic rings of NAADP over time. (C) Pairwise RMSD of NAADP (position normalized with respect to LSM12¹⁻⁸⁰) (D) Favorable interactions between NAADP and LSM residues that are supposed to stabilize for NAADP's binding pose. (E) Distance between favorable pairs of interacting functional groups (see (E)) (F) Distance between the center of mass of the loop (residues 44-53) and the linker (residues 70-75) of LSM12¹⁻⁸⁰. Numbers inside plots represent mean \pm standard deviation of the distance during the corresponding periods indicated by red lines (0-252, 320-670, 670-866, 866-1250, 1350-1900 ns, respectively). (E) starts from 320 ns to omit the initial unstable states. For all distance-time plots, the distance is the rolling average of 10 frames.

3.3.3 Extended Simulation of #14

750 ns extended simulation of #14 revealed a stable binding pose which lasted for about 370 ns (Figure 14 (A-C)). The initial pose obtained from molecular docking at 0 ns already had a relatively close association (14.3 Å) between the loop and the linker and showed favorable electrostatic interactions between Arg72 and the phosphate groups on NAADP and between Lys49 and the carboxyl group (Figure 14 (D; top)). After 250 ns of exploration, NAADP found a stable conformation which lasted until 620 ns, where stable electrostatic interactions were evident for Arg72-purine (arginine-aromatic interaction; (Shah et al., 2012)), Lys42-phosphate and Lys49-carboxyl pairs (Figure 14 (D; bottom)). The Lys49-carboxyl interaction was less stable than the other two pairs, with a higher standard deviation of the distance between the interacting functional groups (Figure 14 (E)). Dissociation of NAADP from LSM12¹⁻⁸⁰ was accompanied by destabilized conformation of NAADP, loss of the three pairs of electrostatic interactions (especially Lys49-carbonyl and Arg72-purine), and opening of the loop-linker groove on LSM12¹⁻⁸⁰ (Figure 14 (B, E, F)).

LSM12¹⁻⁸⁰ and NAADP conformations were extracted at 300.97 ns, and additional two 100 ns simulations were run, both of which successfully reproduced the stable binding at the loop-linker groove and maintained the Arg72-purine, Lys42-phosphate and Lys49-carboxyl interactions. However, similar results were also achieved with two NADP controls.

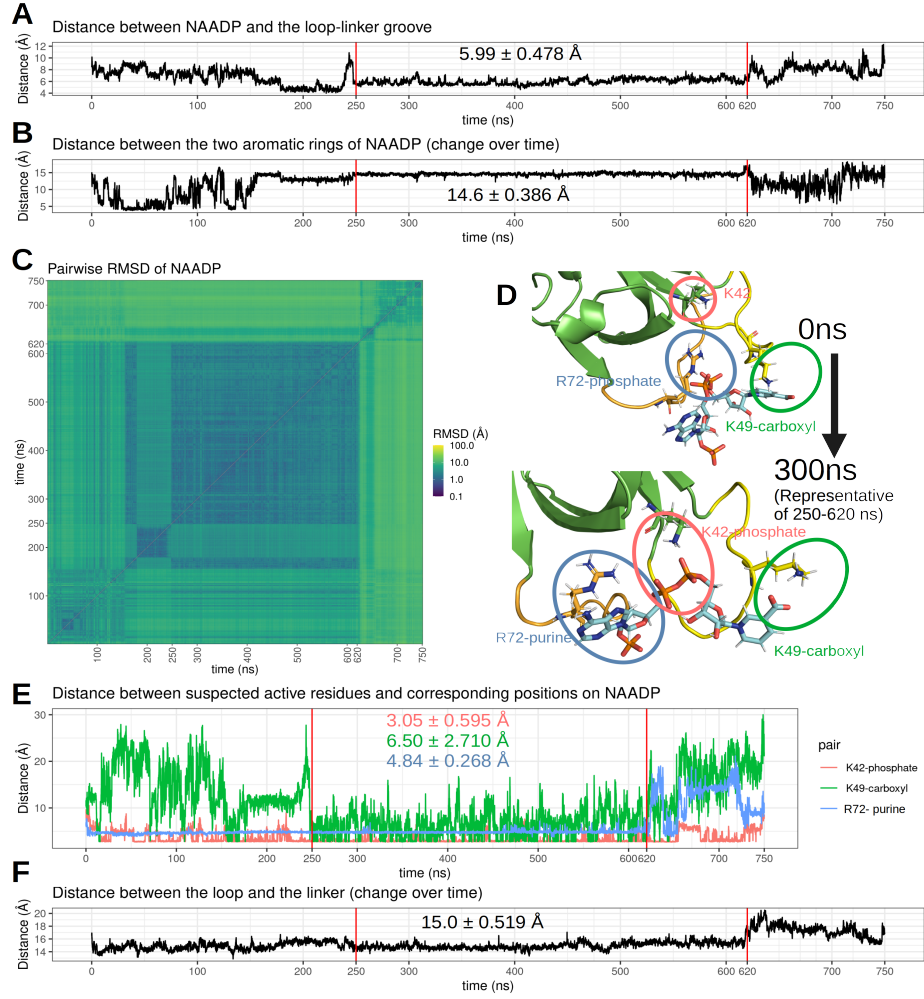


Figure 14: 750 ns extended simulation of #14 revealed a stable binding pose. (A) Distance between the center of mass of NAADP and that of the loop-linker groove over time. **(B)** Distance between the two aromatic rings of NAADP over time. **(C)** Pairwise RMSD of NAADP (position normalized with respect to LSM12¹⁻⁸⁰) **(D)** Favorable interactions between NAADP and LSM residues that are supposed to stabilize for NAADP's binding pose. **(E)** Distance between favorable pairs of interacting functional groups (see (E)) **(F)** Distance between the center of mass of the loop (residues 44-53) and the linker (residues 70-75) of LSM12¹⁻⁸⁰. Numbers inside plots represent mean \pm standard deviation of the distance during the period 250-620 ns. For all distance-time plots, the distance is the rolling average of 10 frames.

3.3.4 De novo binding simulation

The observation of the unbinding and rebinding events (Section 3.3.2) prompted me to assess whether de novo binding of NAADP could be reproduced in MD simulations. 500 ns simulations were performed on systems where the ligand is placed about 40 Å away from the AlphaFold LSM12¹⁻⁸⁰ LSM12¹⁻⁸⁰ structure on the opposite side of the loop-linker groove (Figure 15 (A)).

Both NADP and TPC2-A1-N found their stable binding pose towards the end of the 500 ns simulation. The binding pose of NADP is reminiscent of the stable binding pose of NAADP in #14 (Section 3.3.3), but NADP, which favors the folded conformation (Section 3.1), makes weaker interactions with Arg72 and Lys49 (Figure 15 (B)). TPC2-A1-N induced the formation of a tight binding pocket around it, although it is difficult to assess the contributions from different types of interactions (Figure 15 (C)).

However, NAADP failed to achieve a stable binding pose even when the simulation was extended to 1500 ns (Figure 15 (D)).

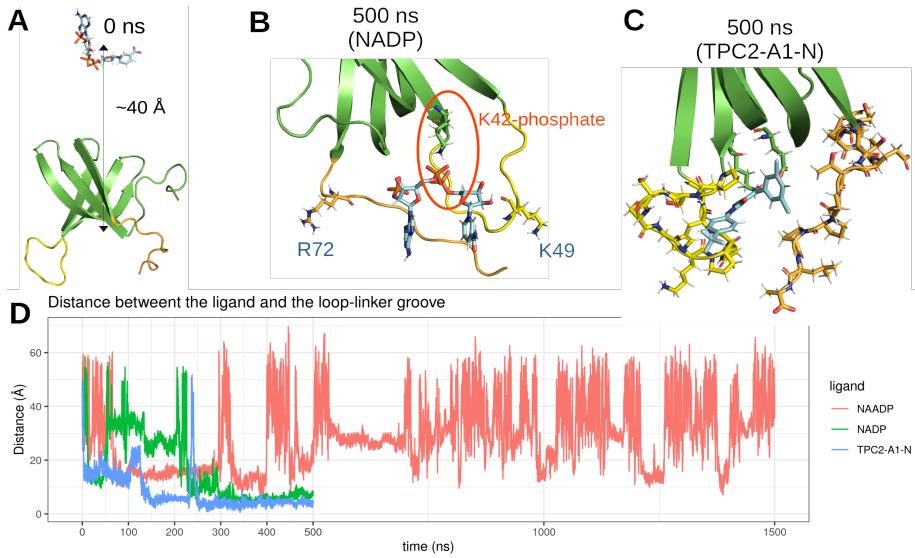


Figure 15: De novo binding simulation of ligands to LSM12¹⁻⁸⁰. (A) Experimental setup. (B) and (C) The binding pose of NADP and TPC2-A1-N at 500 ns. (D) Distance between the center of mass of the ligand and that of the loop-linker groove over time.

3.4 Protein-protein docking

Taufiq Rahman (personal communication, 2021) obtained a TPC2-LSM12 complex from molecular docking using ClusPro, which features 4 electrostatic or

hydrogen bond interactions: D71-K166, S73-K169, E74-R172 and K49-E177 (Figure 16 (A, B)). By specifying these residues as the ‘active residues’, HADDOCK generated TPC2-LSM12¹⁻⁸⁰ complexes with representative stable conformations of LSM12¹⁻⁸⁰ from #14 and #8, that are similar to Figure 16 (A) in overall orientation, but with slightly different residue interactions.

For the LSM12¹⁻⁸⁰ from #14 (HADDOCK score: $-88.4 \text{ kJ mol}^{-1}$), D71-K166 and S73-K169 interactions were largely preserved, but the K49-E177 interaction was lost, as K49 was bound to the carboxyl group of NAADP. E74-R172 was replaced by E74-K283 (Figure 16 (C)). When the NAADP structure, which was unused in protein-protein docking, was aligned, the 2' phosphate group overlapped with E74, suggesting it could instead interact with K283, allowing E74 to interact with R172, as in Rahman’s model (Figure 16 (D)).

For the LSM12¹⁻⁸⁰ from #8 (HADDOCK score: $-116.6 \text{ kJ mol}^{-1}$), D71-K166 and K49-E117 were preserved, S73-K169 was lost D71-K166 and E74-R172 were replaced by E74-K283 (Figure 16 (E)). Alignment of NAADP demonstrated that possible arginine-aromatic interactions (R278-purine) and π -stacking interactions might be made possible by minor translations and bond rotations (Figure 16 (F)).

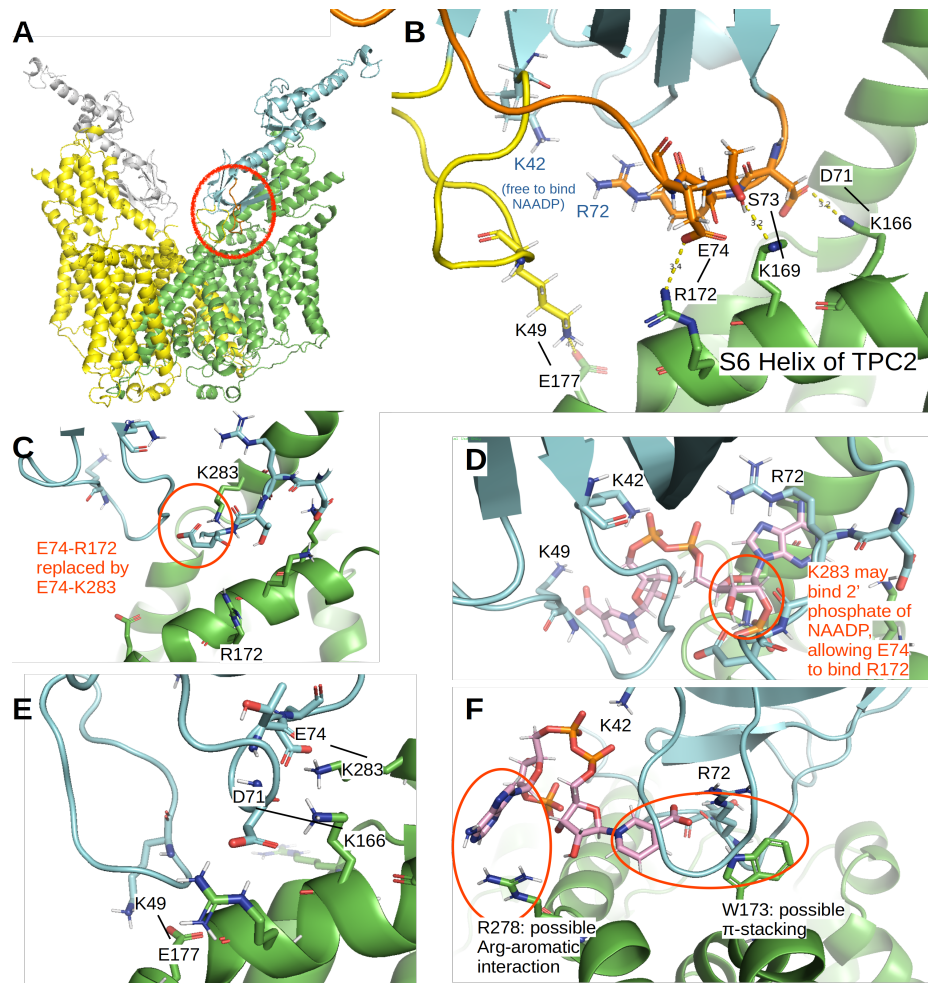


Figure 16: Protein-protein docking of LSM12¹⁻⁸⁰ to TPC2. (A) T. Rahman's docked complex. (B) A zoomed-in view of (A) at the binding site. (C) Docking of LSM12¹⁻⁸⁰ extracted from #14 at 300ns to TPC2. (D) (C) with the NAADP aligned. (E) Docking of LSM12¹⁻⁸⁰ extracted from #8 at 875 ns to TPC2. (F) (E) with the NAADP aligned, viewed from another angle.

Despite the above findings, it is difficult to draw conclusions about how NAADP promotes LSM12 binding to TPC2. While NAADP seemed to promote the association between the loop and the linker and such a short loop-linker distance was observed in these favorable TPC2-LSM12 complexes, the presence of the NAADP in the TPC2-LSM12 binding interface was not taken into account in protein-protein docking experiments.

4 Discussion

LSM12 belongs to the LSM family, in which LSM1-8 are single-domain proteins that usually multimerize into a ring that allows binding of oligonucleotides. As an example, the X-ray structure of *Schizosaccharomyces pombe* LSM1-7 (PDB Code: 6PPQ) (Montemayor et al., 2020) with bound oligonucleotide is shown in (Figure 17 (A)). The properties and functions of larger, often multi-domain LSMs, including LSM12, are elusive, but its experimental size of 22-23 kDa suggests it to function as a monomer (Lin-Moshier et al., 2012; Gunaratne et al., 2019; Zhang et al., 2021). This is supported by the failure of AlphaFold-Multimer (Evans et al., 2022) to predict a plausible dimer, pentamer, hexamer, or heptamer of LSM12 (not shown).

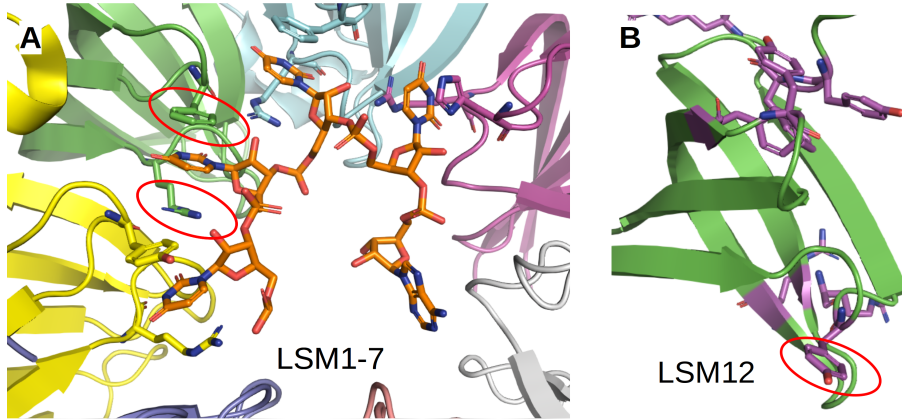


Figure 17: (A) X-ray crystal structure of *Schizosaccharomyces pombe* LSM1-7. (B) Human LSM12¹⁻⁸⁰ in a similar orientation as the green LSM subunit in (A). Arginines and aromatic residues are colored purple.

The binding pose of NAADP in LSM12 is likely to be different from that of oligonucleotides in LSM1-7. In the latter case, each base is surrounded by an aromatic residue and a arginine residue, forming stable π stacking interactions. To produce an equivalent conformation, the dinucleotide NAADP would require a dimer that LSM12 would not form, and LSM12 lacks the arginine-aromatic residue pair at the equivalent positions (Figure 17 (B)).

Although many of the results presented here support the hypothesis that NAADP binds to the loop-linker groove via an induced-fit mechanism, they should be viewed with caution due to the lack of repeats and lack of reproducibility in the case of #8. The inconsistency of the behavior of NAADP might stem from the inconsistent parameterization of the ligand. While the force field parameters for common biological molecules especially proteins are widely tested and fine-tuned with reference to experimental data, the parameters

generated for new small molecules are not always accurate. Although I have roughly checked that the charges and bond lengths were reasonable, they did vary slightly even when the same molecule with the same conformation was being used, and the discrepancy increases when different conformations of the same molecule were used. For example, the original extended conformation always used the parameters generated with the NAADP conformation at 0 ns, but when repeats are performed on the extracted conformation at 300 ns, they used the parameters newly generated from the conformation at 300ns, which are different from the original ones.

In the case of #14, although two 100 ns simulations of NADP showed similar association to the loop-linker groove as in the case of NAADP, there were too few repeats, and the simulation times are too short. Otherwise, the involvement of the carboxyl group possessed by NAADP and NADP could explain their different affinity to LSM12. Future experiments could repeatedly measure the time to reach a certain RMSD threshold starting from a supposed stable binding pose, for example, in order to draw statistically significant conclusions about the difference in the stability between NAADP and NADP at the binding site.

Lack of experimental data also prevented conclusions to be made regarding the actual binding pose of NAADP on LSM12 and that of LSM12 on TPC2. Yet, the recurrent involvement of a few residues, especially R72, K42 and K49, in both NAADP binding and TPC2 binding makes them desirable targets for mutagenesis studies both *in vivo* and *in silico* in future studies. The most direct approach to confirm the binding pose would be to purify the LSM12¹⁻⁸⁰-NAADP complex and obtain a structure by X-ray crystallography or cryo-EM. Though such structural biology approaches can be laborious, establishing the accurate binding mode of NAADP to this prototypical NAADP-binding protein may accelerate the studies on the mechanisms of other NAADP-binding proteins, including JPT2 in humans and the unidentified ~41 kDa protein in sea urchins.

The conformation sampling method and scoring function used in this study were suboptimal in predicting the bind mode of NAADP. With the expanding repertoire of experimentally solved ligand-protein interactions, empirical based scoring functions, especially those powered by machine learning, are becoming more accurate and often outperform the classical force field-based methods such as Amber MM/GBSA used in this study (Li et al., 2021). Such scoring functions may be able to more accurately identify promising binding poses of NAADP.

A lot remains to be done in order to rationalize how LSM12-NAADP operates on TPC2. While LSM12 was predicted to form favorable interactions with the S6 helix in protein-protein docking experiments, which is in agreement with the finding that LSM12 competitively inhibits PI(3,5)P₂ (Du et al., 2022), the exact gate opening mechanism, and more importantly the ion selectivity switching mechanism still remain elusive. The methods used by She et al. (2019) to resolve human TPC2 structure in the apo state and PI(3,5)P₂-bound states by cryo-EM might be modified to resolve the TPC2-LSM12 complex, and knowledge gained from MD studies on K⁺ and Na⁺ conductivity and gating mechanisms

(DeMarco et al., 2019) may also be adapted to elucidate the mechanisms of TPC2.

References

- Aarhus R, Graeff RM, Dickey DM, Walseth TF and Hon CL (1995). ADP-ribosyl cyclase and CD38 catalyze the synthesis of a calcium-mobilizing metabolite from NADP⁺. *Journal of Biological Chemistry.* **270**(51):30327–30333.
- Abraham MJ, Murtola T, Schulz R, Pál S, Smith JC, Hess B and Lindahl E (2015). GROMACS: High performance molecular simulations through multi-level parallelism from laptops to supercomputers. *SoftwareX.* **1–2**:19–25.
- Alharbi AF and Parrington J (2019). Endolysosomal Ca²⁺ signaling in cancer: The role of TPC2, from tumorigenesis to metastasis. *Frontiers in Cell and Developmental Biology.* **7**.
- Alharbi AF and Parrington J (2021). Deciphering the Role of Endolysosomal Ca²⁺ Channels in Immunity. *Frontiers in Immunology.* **12**:2021.656965.
- Bak B J. (2001). NAADP receptors are present and functional in the heart. *Current Biology.* **11**(12):987–990.
- Berendsen HJC, Postma JPM, Gunsteren WF van, DiNola A and Haak JR (1984). Molecular dynamics with coupling to an external bath. *The Journal of Chemical Physics.* **81**(8):3684–3690.
- Berg I, Potter BVL, Mayr GW and Guse AH (2000). Nicotinic acid adenine dinucleotide phosphate (NAADP⁺) is an essential regulator of t-lymphocyte Ca²⁺-signaling. *Journal of Cell Biology.* **150**(3):581–588.
- Boccaccio A, Scholz-Starke J, Hamamoto S, Larisch N, Festa M, Gutla PVK, Costa A, Dietrich P, Uozumi N and Carpaneto A (2014). The phosphoinositide PI(3,5)P2 mediates activation of mammalian but not plant TPC proteins: Functional expression of endolysosomal channels in yeast and plant cells. *Cellular and Molecular Life Sciences.* **71**(21):4275–4283.
- Brailoiu E, Churamani D, Cai X, Schrlau MG, Brailoiu GC, Gao X, Hooper R, Boulware MJ, Dun NJ, Marchant JS and Patel S (2009). Essential requirement for two-pore channel 1 in NAADP-mediated calcium signaling. *Journal of Cell Biology.* **186**(2):201–209.
- Bussi G, Donadio D and Parrinello M (2007). Canonical sampling through velocity rescaling. *Journal of Chemical Physics.* **126**(1):014101.
- Calcraft PJ, Ruas M, Pan Z, Cheng X, Arredouani A, Hao X, Tang J, Rietdorf K, Teboul L, Chuang K-T, Lin P, Xiao R, Wang C, Zhu Y, Lin Y, Wyatt CN, Parrington J, Ma J, Evans AM, Galione A, et al. (2009). NAADP mobilizes calcium from acidic organelles through two-pore channels. *Nature.* **459**(7246):596–600.
- Cancela JM, Churchill GC and Galione A (1999). Coordination of agonist-induced Ca²⁺-signalling patterns by NAADP in pancreatic acinar cells. *Na-*

ture. **398**(6722):74–76.

Churamani D, Carrey EA, Dickinson GD and Patel S (2004). Determination of cellular nicotinic acid-adenine dinucleotide phosphate (NAADP) levels. *Biochemical Journal*. **380**(2):449–454.

Cosker F, Cheviron N, Yamasaki M, Menteyne A, Lund FE, Moutin M-J, Galione A and Cancela J-M (2010). The Ecto-enzyme CD38 Is a Nicotinic Acid Adenine Dinucleotide Phosphate (NAADP) Synthase That Couples Receptor Activation to Ca²⁺ Mobilization from Lysosomes in Pancreatic Acinar Cells. *Journal of Biological Chemistry*. **285**(49):38251–38259.

DeMarco KR, Bekker S and Vorobyov I (2019). Challenges and advances in atomistic simulations of potassium and sodium ion channel gating and permeation. *Journal of Physiology*. **597**(3):679–698.

Du C, Shah KR and Yan J (2022). Lsm12, an NAADP receptor, is also a PI(3,5)P₂-competitive antagonist of human two pore channels. *Biophysical Journal*. **121**(3):244a.

Evans R, O'Neill M, Pritzel A, Antropova N, Senior A, Green T, Žídek A, Bates R, Blackwell S, Yim J, Ronneberger O, Bodenstein S, Zielinski M, Bridgland A, Potapenko A, Cowie A, Tunyasuvunakool K, Jain R, Clancy E, Kohli P, et al. (2022). Protein complex prediction with AlphaFold-multimer. *bioRxiv*.

Fang C, Li T, Li Y, Xu GJ, Deng QW, Chen YJ, Hou YN, Lee HC and Zhao YJ (2018). CD38 produces nicotinic acid adenosine dinucleotide phosphate in the lysosome. *Journal of Biological Chemistry*. **293**(21):8151–8160.

Genheden S and Ryde U (2015). The MM/PBSA and MM/GBSA methods to estimate ligand-binding affinities. *Expert Opinion on Drug Discovery*. **10**(5):449–461.

Gerndt S, Chen C-C, Chao Y-K, Yuan Y, Burgstaller S, Rosato AS, Krogsaeter E, Urban N, Jacob K, Nguyen ONP, Miller MT, Keller M, Vollmar AM, Gudermann T, Zierler S, Schredelseker J, Schaefer M, Biel M, Malli R, Wahlschott C, et al. (2020). Agonist-mediated switching of ion selectivity in TPC2 differentially promotes lysosomal function. *eLife*. **9**:54712.

Grimm C, Holdt LM, Chen C-C, Hassan S, Müller C, Jörs S, Cuny H, Kissing S, Schröder B, Butz E, Northoff B, Castonguay J, Luber CA, Moser M, Spahn S, Lüllmann-Rauch R, Fendel C, Klugbauer N, Griesbeck O, Haas A, et al. (2014). High susceptibility to fatty liver disease in two-pore channel 2-deficient mice. *Nature Communications*. **5**:4699.

Gu F, Krüger A, Roggenkamp HG, Alpers R, Lodygin D, Jaquet V, Möckl F, Lola C, Hernandez C, Winterberg K, Bauche A, Rosche A, Grasberger H, Kao JY, Schetelig D, Werner R, Schröder K, Cartt M, Bowie AG, Huber S, Meier C, et al. (2021). Dual NADPH oxidases DUOX1 and DUOX2 synthesize NAADP and are necessary for Ca²⁺ signaling during T cell activation. *Science Signaling*. **14**(709):eabe3800.

- Guedes IA, Pereira FSS and Dardenne LE (2018). Empirical scoring functions for structure-based virtual screening: Applications, critical aspects, and challenges. *Frontiers in Pharmacology*. **9**.
- Gunaratne GS, Brailoiu E, He S, Unterwald EM, Patel S, Slama JT, Walseth TF and Marchant JS (2021). Essential requirement for JPT2 in NAADP-evoked Ca^{2+} signaling. *Science Signaling*. **14**(675):eabd5605.
- Gunaratne GS, Su P, Marchant JS, Slama JT and Walseth TF (2019). 5-azido-8-ethynyl-NAADP: A bifunctional, clickable photoaffinity probe for the identification of NAADP receptors. *Biochimica et Biophysica Acta (BBA) - Molecular Cell Research*. **1866**(7):1180–1188.
- Guo J, Zeng W and Jiang Y (2017). Tuning the ion selectivity of two-pore channels. *Proceedings of the National Academy of Sciences*. **114**(5):1009–1014.
- Guse AH (2022). NAADP signaling: New kids on the block. *Cells*. **11**(6):1054.
- Hockey LN, Kilpatrick BS, Eden ER, Lin-Moshier Y, Brailoiu GC, Brailoiu E, Futter CE, Schapira AH, Marchant JS and Patel S (2015). Dysregulation of lysosomal morphology by pathogenic LRRK2 is corrected by TPC2 inhibition. *Journal of Cell Science*. **128**(2):232–238.
- Ishibashi K, Suzuki M and Imai M (2000). Molecular cloning of a novel form (two-repeat) protein related to voltage-gated sodium and calcium channels. *Biochemical and Biophysical Research Communications*. **270**(2):370–376.
- Jorgensen WL, Chandrasekhar J, Madura JD, Impey RW and Klein ML (1983). Comparison of simple potential functions for simulating liquid water. *The Journal of Chemical Physics*. **79**(2):926–935.
- Jumper J, Evans R, Pritzel A, Green T, Figurnov M, Ronneberger O, Tunyasuvanakool K, Bates R, Žídek A, Potapenko A, Bridgland A, Meyer C, Kohl SAA, Ballard AJ, Cowie A, Romera-Paredes B, Nikolov S, Jain R, Adler J, Back T, et al. (2021). Highly accurate protein structure prediction with AlphaFold. *Nature*. **596**(7873):583–589.
- Kinnear NP, Boittin F-X, Thomas JM, Galione A and Evans AM (2004). Lysosome-sarcoplasmic reticulum junctions: A trigger zone for calcium signaling by nicotinic acid adenine dinucleotide phosphate and endothelin-1. *Journal of Biological Chemistry*. **279**(52):54319–54326.
- Korb O, Stützle T and Exner TE (2006). PLANTS: Application of ant colony optimization to structure-based drug design. In: Dorigo M, Gambardella L M, Birattari M, Martinoli A, Poli R, and Stützle T, eds. *Ant Colony Optimization and Swarm Intelligence*. Springer Berlin Heidelberg. Berlin, Heidelberg: 247–258.
- Leach AR and Leach AR (2001). *Molecular Modelling: Principles and Applications*. Pearson education.

- Lee HC and Aarhus R (1995). A derivative of NADP mobilizes calcium stores insensitive to inositol trisphosphate and cyclic ADP-ribose. *Journal of Biological Chemistry*. **270**(5):2152–2157.
- Li H, Sze K-H, Lu G and Ballester PJ (2021). Machine-learning scoring functions for structure-based virtual screening. *WIREs Computational Molecular Science*. **11**(1):e1478.
- Lin-Moshier Y, Walseth TF, Churamani D, Davidson SM, Slama JT, Hooper R, Brailoiu E, Patel S and Marchant JS (2012). Photoaffinity labeling of nicotinic acid adenine dinucleotide phosphate (NAADP) targets in mammalian cells. *Journal of Biological Chemistry*. **287**(4):2296–2307.
- Luan S and Wang C (2021). Calcium Signaling Mechanisms Across Kingdoms. *Annual Review of Cell and Developmental Biology*. **37**(1):311–340.
- Maier JA, Martinez C, Kasavajhala K, Wickstrom L, Hauser KE and Simmerling C (2015). ff14SB: Improving the accuracy of protein side chain and backbone parameters from ff99SB. *Journal of Chemical Theory and Computation*. **11**(8):3696–3713.
- Meng X-Y, Zhang H-X, Mezei M and Cui M (2011). Molecular docking: A powerful approach for structure-based drug discovery. *Current Computer-Aided Drug Design*. **7**(2):146–157.
- Michaud-Agrawal N, Denning EJ, Woolf TB and Beckstein O (2011). MDAnalysis: A toolkit for the analysis of molecular dynamics simulations. *Journal of Computational Chemistry*. **32**(10):2319–2327.
- Montemayor EJ, Virta JM, Hayes SM, Nomura Y, Brow DA and Butcher SE (2020). Molecular basis for the distinct cellular functions of the Lsm1-7 and Lsm2-8 complexes. *RNA*. **26**(10):1400–1413.
- Morgan AJ, Davis LC and Galione A (2015). Imaging approaches to measuring lysosomal calcium. *Methods in Cell Biology*. Academic Press. Cambridge, MA, USA: 159–195.
- Morgan AJ and Galione A (2008). Investigating cADPR and NAADP in intact and broken cell preparations. *Methods*. **46**(3):194–203.
- O’Boyle NM, Banck M, James CA, Morley C, Vandermeersch T and Hutchison GR (2011). Open babel: An open chemical toolbox. *Journal of Cheminformatics*. **3**(1):33.
- Ogunbayo OA, Duan J, Xiong J, Wang Q, Feng X, Ma J, Zhu MX and Evans AM (2018). mTORC1 controls lysosomal Ca^{2+} release through the two-pore channel TPC2. *Science Signaling*. **11**(525):eaao5775.
- Pandey V, Chuang C-C, Lewis AM, Aley PK, Brailoiu E, Dun NJ, Churchill GC and Patel S (2009). Recruitment of NAADP-sensitive acidic Ca^{2+} stores by glutamate. *Biochemical Journal*. **422**(3):503–512.

- Parrinello M and Rahman A (1981). Polymorphic transitions in single crystals: A new molecular dynamics method. *Journal of Applied Physics*. **52**(12):7182–7190.
- Patel S and Kilpatrick BS (2018). Two-pore channels and disease. *Biochimica et Biophysica Acta (BBA) - Molecular Cell Research*. **1865**(11, Part B):1678–1686.
- Raffaello A, Mammucari C, Gherardi G and Rizzuto R (2016). Calcium at the Center of Cell Signaling: Interplay between Endoplasmic Reticulum, Mitochondria, and Lysosomes. *Trends in Biochemical Sciences*. **41**(12):1035–1049.
- Rahman T, Cai X, Brailoiu GC, Abood ME, Brailoiu E and Patel S (2014). Two-pore channels provide insight into the evolution of voltage-gated Ca^{2+} and Na^+ channels. *Science Signaling*. **7**(352):ra109.
- Roggenkamp HG, Khansahib I, Hernandez C, LC, Zhang Y, Lodygin D, Krüger A, Gu F, Möckl F, Löhdorf A, Wolters V, Woike D, Rosche A, Bauche A, Schetelig D, Werner R, Schlüter H, Failla AV, Meier C, Fliegert R, Walseth TF, et al. (2021). HN1L/JPT2: A signaling protein that connects NAADP generation to Ca^{2+} microdomain formation. *Science Signaling*. **14**(675):eabd5647.
- Ruas M, Davis LC, Chen C-C, Morgan AJ, Chuang K-T, Walseth TF, Grimm C, Garnham C, Powell T, Platt N, Platt FM, Biel M, Wahl-Schott C, Parrington J and Galione A (2015). Expression of Ca^{2+} -permeable two-pore channels rescues NAADP signalling in TPC-deficient cells. *The EMBO Journal*. **34**(13):1743–1758.
- Santella L, Kyozuka K, Genazzani AA, De Riso L and Carafoli E (2000). Nicotinic acid adenine dinucleotide phosphate-induced $\text{ca}(2+)$ release. Interactions among distinct $\text{ca}(2+)$ mobilizing mechanisms in starfish oocytes. *J Biol Chem*. **275**(12):8301–8306.
- Shah D, Li J, Shaikh AR and Rajagopalan R (2012). Arginine–aromatic interactions and their effects on arginine-induced solubilization of aromatic solutes and suppression of protein aggregation. *Biotechnology Progress*. **28**(1):223–231.
- She J, Guo J, Chen Q, Zeng W, Jiang Y and Bai X (2018). Structural insights into the voltage and phospholipid activation of the mammalian TPC1 channel. *Nature*. **556**(7699):130–134.
- She J, Zeng W, Guo J, Chen Q, Bai X and Jiang Y (2019). Structural mechanisms of phospholipid activation of the human TPC2 channel. *eLife*. **8**:e45222.
- Soares S, Thompson M, White T, Isbell A, Yamasaki M, Prakash Y, Lund FE, Galione A and Chini EN (2007). NAADP as a second messenger: Neither CD38 nor base-exchange reaction are necessary for in vivo generation of

- NAADP in myometrial cells. *American Journal of Physiology-Cell Physiology*. **292**(1):C227–C239.
- Sousa da Silva AW and Vranken WF (2012). ACPYPE - AnteChamber PYthon parser interface. *BMC Research Notes*. **5**(1):367.
- Terrar DA (2022). Endolysosomal calcium release and cardiac physiology. *Cell Calcium*. **104**:102565.
- Varadi M, Anyango S, Deshpande M, Nair S, Natassia C, Yordanova G, Yuan D, Stroe O, Wood G, Laydon A, Žídek A, Green T, Tunyasuvunakool K, Petersen S, Jumper J, Clancy E, Green R, Vora A, Lutfi M, Figurnov M, et al. (2022). AlphaFold protein structure database: Massively expanding the structural coverage of protein-sequence space with high-accuracy models. *Nucleic Acids Research*. **50**(D1):D439–D444.
- Walseth TF and Guse AH (2021). NAADP: From discovery to mechanism. *Frontiers in Immunology*. **12**:703326.
- Wang J, Wolf RM, Caldwell JW, Kollman PA and Case DA (2004). Development and testing of a general amber force field. *Journal of Computational Chemistry*. **25**(9):1157–1174.
- Wang X, Zhang X, Dong X, Samie M, Li X, Cheng X, Goschka A, Shen D, Zhou Y, Harlow J, Zhu MX, Clapham DE, Ren D and Xu H (2012). TPC Proteins Are Phosphoinositide- Activated Sodium-Selective Ion Channels in Endosomes and Lysosomes. *Cell*. **151**(2):372–383.
- Wickham H (2016). *Ggplot2: Elegant Graphics for Data Analysis*. Springer.
- Yamasaki M, Masgrau R, Morgan AJ, Churchill GC, Patel S, Ashcroft SJH and Galione A (2004). Organelle selection determines agonist-specific Ca^{2+} signals in pancreatic acinar and cells. *Journal of Biological Chemistry*. **279**(8):7234–7240.
- Yang J, Zhao Z, Gu M, Feng X and Xu H (2019). Release and uptake mechanisms of vesicular Ca^{2+} stores. *Protein & Cell*. **10**(1):8–19.
- Yasuteru S, A. KA, Cheng-Chang C, W. TM, E. BW, Norbert K, Christian G, Christian W-S, Martin B and A. DR (2015). Two-pore channels control ebola virus host cell entry and are drug targets for disease treatment. *Science*. **347**(6225):995–998.
- Zhang J, Guan X, Shah K and Yan J (2021). Lsm12 is an NAADP receptor and a two-pore channel regulatory protein required for calcium mobilization from acidic organelles. *Nature Communications*. **12**(1):4739.
- Zondlo NJ (2013). Aromatic–proline interactions: Electronically tunable CH/π interactions. *Accounts of Chemical Research*. **46**(4):1039–1049.
- Zong X, Schieder M, Cuny H, Fenske S, Gruner C, Rötzer K, Griesbeck O, Harz H, Biel M and Wahl-Schott C (2009). The two-pore channel TPCN2

mediates NAADP-dependent Ca^{2+} -release from lysosomal stores. *Pflügers Archiv - European Journal of Physiology*. **458**(5):891–899.

Zundert GCP van, Rodrigues JPGLM, Trellet M, Schmitz C, Kastritis PL, Karaca E, Melquiond ASJ, Dijk M van, Vries SJ de and Bonvin AMJJ (2016). The HADDOCK2.2 web server: User-friendly integrative modeling of biomolecular complexes. *Journal of Molecular Biology*. **428**(4):720–725.